Draft

November 9, 2001

Muon Identification in the Belle Experiment at KEKB

A. Abashian[8], K. Abe[3], K. Abe[6], P. K. Behera[7], F. Handa[6], T. Iijima[3], Y. Inoue[5], H. Miyake[4], T. Nagamine[6], E. Nakano[5], S. Narita[6,†], L. Piilonen[8], S. Schrenk[1], Y. Teramoto[5], K. Trabelsi[2], J. G. Wang[8], M. Yamaga[6], A. Yamaguchi[6], and Y. Yusa[5]

[1] *Department of Physics, University of Cincinnati, Cincinnati OH 33333, U.S.A.*

[2] *Department of Physics and Astronomy, University of Hawaii, Honolulu HI 96822, U.S.A.*

[3] *KEK, High Energy Accelerator Research Organization, Tsukuba, Ibaraki 305-0801, Japan*

[4] *Department of Physics, Osaka University, Osaka 560-0043, Japan*

[5] *Institute for Cosmic Ray Physics, Osaka City University, Osaka 558-8585, Japan*

[6] *Department of Physics, Tohoku University, Sendai 980-8578, Japan*

[7] *Utkal University, Bhubaneswer-751 004, India*

[8] *Department of Physics, Virginia Polytechnic Institute and State University, Blackburg VA 24061, U.S.A.*

[†]Present address: Department of Electrical and Electronic Engineering, Iwate University, Iwate 020-8551, Japan

Abstract

This paper describes the muon identification method and its performance in the Belle experiment at KEKB. Muon and hadron likelihood are calculated for each track using its range and transverse scattering in the K_L-and-muon detector (KLM). We apply a cut on the normalized muon likelihood $\mathcal{L}_\mu$ to identify the track as a muon. Above the

detection threshold of 0.6 GeV/c, the measured muon detection efficiency and pion fake rate are approximately constant for momenta greater than 1.0 GeV/c and 1.5 GeV/c, respectively. Between 1.0 and 3.0 GeV/c, the averaged muon detection efficiency is 89% and the pion fake rate per track is 1.4% over the KLM acceptance, using the standard selection criterion $\mathcal{L}_\mu > 0.9$.

Key words: Muon identification, Belle detector, KEKB

PACS: 29.50.+v

1 Introduction

Experimental studies of the weak interaction are important to understand the Standard Model and to find signatures of new physics. The Belle detector [1] is designed to measure CP nonconservation in the decays of B mesons emitted coherently in pairs from the disintegration of the $\Upsilon(4S)$ resonance that is produced in asymmetric e^+e^- collisions at the KEK B factory (KEKB) [2]. Belle also studies other properties of B mesons, charm hadrons, τ leptons, and two-photon interactions that are produced concurrently in the e^+e^- collisions.

Leptons in Belle are used primarily in the reconstruction of charmonium daughters (J/ψ, ψ', η_c, χ_c) from CP-sensitive decays of the B meson, and to tag the flavor of the partner B meson that is produced coherently via $\Upsilon(4S) \to B\overline{B}$ in the same event.[3] For example, in the golden decay mode[4] $B^0 \to J/\psi\, K_S \to (\ell^+\ell^-)\,(\pi^+\pi^-)$, the J/ψ meson is reconstructed

from its lepton daughters and the partner's B flavor can be tagged by the charge of its lepton daughter.

The momentum range for good muon identification is $1.0 < p < 3.0$ GeV/c. The leptons that arise from the decays of B mesons and charm hadrons have momenta below about 3.0 GeV/c. Muons need at least 0.6 GeV/c to reach the muon-and-K_L (KLM) detector [5] outside Belle's solenoid. For high hadron rejection ($< 2\%$), a passage of half the KLM detector is required, which set 1.0 GeV/c.

In this report, we describe briefly the Belle detector in Section 2. We present the muon identification method and its performance in Sections 3 and 4, respectively.

2 Belle detector

The Belle detector consists of a three-layer silicon vertex detector (SVD), a 50-layer central drift chamber (CDC), an array of 1188 aerogel Cerenkov counters (ACC), 128 time-of-flight scintillation counters (TOF), an electromagnetic calorimeter containing 8736 CsI(Tℓ) crystals (ECL), and the K_L-and-muon detector (KLM), listed in order of radial distance from the interaction point. All but the KLM are contained in a superconducting solenoid with a central magnetic field of 1.5 T. The fourteen 4.7-cm thick iron absorber plates of the KLM also serve as the solenoid's return yoke.

The side view of the Belle detector is shown in Fig. 1. The origin is at crossing point of the 8.5 GeV electron beam and the 3.0 GeV positron beam, displaced along the beam axis from the geometric center of the detector to account for the boost of the center of momentum relative to the laboratory frame of reference. The horizontal z axis lies along the positron beam[1], with the positrons moving along $-z$. The orthogonal x axis is also in the horizontal plane, with $+x$ pointing away from the center of the accelerator ring. The y axis is along the vertical, to complete a right-handed coordinate frame. The polar angle θ is measured from the $+z$ axis, while the azimuthal angle ϕ is measured counterclockwise from the $+x$ axis in the xy plane. The radial distance r is measured from the z axis.

We describe the CDC and KLM in more detail next, since these are the two detectors used in muon identification.

The CDC's 50 cylindrical drift cell layers are organized into 11 superlayers [6], with each superlayer containing between three and six either axial or small-angle-stereo layers. Its polar angle coverage is $17^\circ < \theta < 150^\circ$. Charged particle tracks are reconstructed from the hits in the CDC and, if possible, are projected into and matched with hits in the SVD. The resolution in transverse momentum $p_{\rm T}$ is $\sqrt{(0.19p_{\rm T})^2 + (0.41/\beta)^2}$ % for tracks with SVD hits and $\sqrt{(0.34p_{\rm T})^2 + (0.41/\beta)^2}$ % otherwise. Here, β is the velocity of the particle.

The KLM comprises the octagonal-shaped barrel and two endcap regions. The detector

[1]The electron beam is tilted 22 mrad from the positron beam in the novel crossing scheme of KEKB.

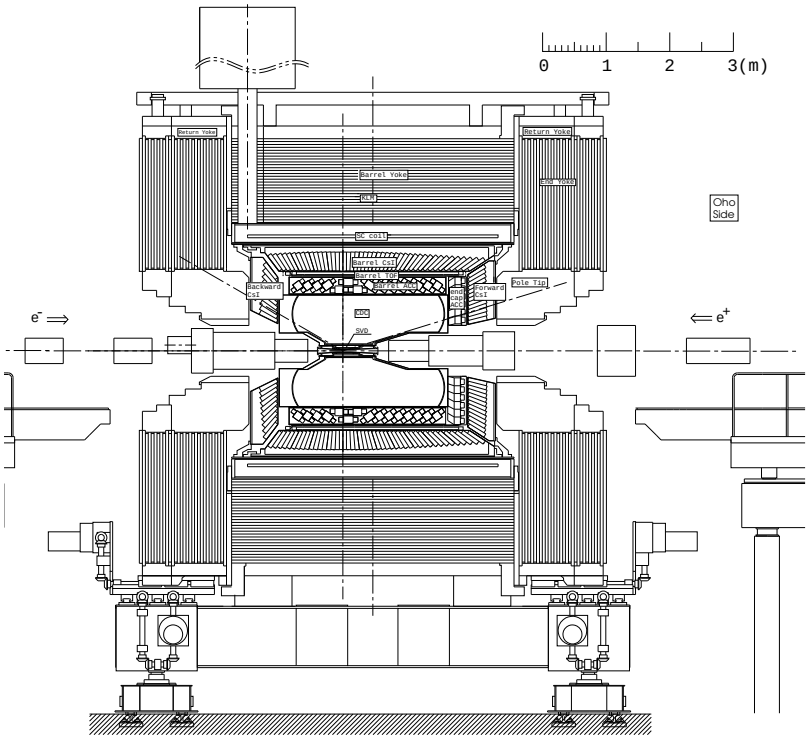

Figure 1: Belle detector.

consists of alternating layers of 3.7-cm thick glass-electrode resistive plate chamber (RPC) modules and 4.7 cm thick iron plates. The barrel has 15 modules with 14 iron plates, and each endcap has 14 modules with 14 iron plates. The modules are rectangular in the barrel (2 per octant layer) and fan-shaped (4 per layer) in the endcap. The barrel region covers the polar angular range from 51° to 117°; the two endcaps extend this coverage to between 25° and 145°. The iron plates provide a total of 3.9 interaction lengths of material for a hadron crossing at normal incidence; this is in addition to the 0.8 interaction lengths of the ECL.

Each RPC module contains two independent RPCs arranged back-to-back, sandwiched between orthogonal readout strip planes. This redundant superlayer design provides a 3D measurement of the coordinates of a throughgoing charged track with better than 98% efficiency, since a streamer that develops in either RPC will induce an image charge on both readout strip planes. The time resolution of the RPC signals is a few nanoseconds.

The rectangular z- and ϕ-view readout strips in the barrel are roughly 5 cm wide. The θ-view readout strips in the endcap are 3.6 cm wide coaxial arcs, while the ϕ-view readout strips are radial trapezoids of width 1.9 cm at the inner radius of 130.5 cm and 4.7 cm at the outer radius of 331.0 cm. There are a total of 38,000 readout strips in the system.

The ECL can be used as an independent high-efficiency muon identifier by requiring an energy deposit of between 0.1 and 0.3 GeV for a throughgoing charged track, straddling the typical minimum-ionizing deposit of 0.17 GeV. This is most useful in cases such as J/ψ reconstruction where kinematic cuts can compensate for the inherently high hadron fake rate.

3 Muon Identification Method

3.1 Introduction

Muon identification begins with the reconstruction of a charged track in the CDC with matching SVD hits, and continues with its extrapolation through the outer detectors to its stopping point or its escape from the detector. A track is considered to be within the KLM acceptance if it crosses at least one RPC layer; this requires at least 0.6 GeV/c of momentum. If an RPC hit is found near the crossing of the extrapolated track and a KLM layer, the hit is associated with the track. The outermost layer crossed by the extrapolated track defines the predicted range of the track assuming the track has no hadronic interaction with the materials. The actual range of the track is measured by the outermost layer with an associated RPC hit. Because most tracks in the events of interest are hadronic, we discard those whose predicted and measured ranges differ substantially (prerejection). The remaining tracks are re-extrapolated, now using a Kalman filtering/fitting technique to steer each track as it is swum through the KLM. The difference between the predicted and measured ranges and the goodness of fit of the transverse deviations of the associated hits from the re-extrapolated crossings provide the two variables used in a likelihood ratio to test the hypothesis that the track resembles a muon rather than a charged hadron.

3.2 Track extrapolation

A helical track, reconstructed in the CDC, is refined by a Kalman filter to determine the helix parameters near the outermost layer of CDC, assuming the track is one of five common charged particles (e, μ, π, K, p). The helix parameterization is justified by the uniformity of the solenoidal magnetic field within the tracking volume and the small energy loss of the track within the CDC. The helix parameters and their associated errors at the outermost CDC layer are converted to 3D point and slope vector format and then swum outward using GEANT3 [8]. The extrapolation uses the pion hypothesis since this is the most common charged particle encountered in the events of interest. Note that the track extrapolation is used in the analysis of the ACC, TOF and ECL signals besides muon identification in the KLM. Only ionization energy loss and multiple Coulomb scattering are modeled in this blind extrapolation. The mean ionization energy loss reduces the track's energy as it swims, while the fluctuations in energy loss and the multiple scattering enlarge its uncertainties.

GEANT3 uses a uniform solenoidal field inside the superconducting coil ($r < 180$ cm), except near the two ends of the interaction region ($r < 15$ cm and $z < -50$ cm or $z > 80$ cm) where the field deviates by 2–3 % because of the beamline magnets. Within the plates of the iron return yoke, the non-uniform field's radial and axial components are determined by table lookup from a POISSON [9] calculation to 10 % accuracy. The very small residual field (< 10 Gauss) in the inter-plate gaps of the KLM is set to zero.

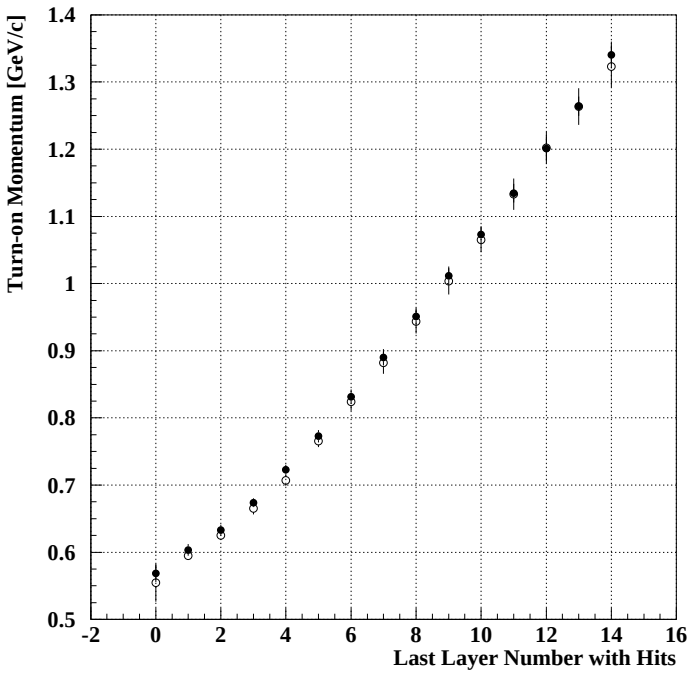

Figure 2: *Turn-on momentum at each KLM layer for real (closed circles) and simulated (open circles) muons.*

We tested the fidelity of the detector model (materials and their geometries) used by GEANT3 by measuring the "turn-on momentum" for each KLM layer, the minimum momentum needed to produce a hit in the layer. Figure 2 shows the turn-on momenta for real and simulated muons. Incorrect thicknesses or compositions of materials, or missing materials, would appear as a difference between the two curves. The discrepancy is less than 8 MeV, which is less than 14 % of one iron layer at 1 GeV/c.

Detection efficiency of the RPCs is measured using the reaction $e^+e^- \to \mu^+\mu^-$. The extracted efficiencies are tabulated in a two-dimensional grid with a cell size of 4×4 readout

strip units. These efficiencies are used in the Monte Carlo simulation of the Belle detector, and thereby match the actual response of the KLM RPCs to throughgoing charged tracks. The probability density functions, used to calculate muon likelihood, are updated whenever a significant change occurs in these RPC efficiencies.

3.3 KLM hit reconstruction

In a KLM module, the signals induced on the orthogonal readout strips by the streamer that forms in the RPC gas gap along the throughgoing particle's trajectory are digitized by discriminators and encoded into a time-multiplexed stream by a circuit based on programmable gate arrays. This stream is recorded in a multihit Fastbus TDC (LeCroy 1877) upon receipt of a trigger signal indicative of an interesting event in the Belle detector. The time-multiplexed stream is later decoded into the hits on a group of 12 adjacent readout strips. Hits outside the event time window of 1.0 μs are discarded.

Contiguous in-time readout strips are grouped into a one-dimensional (1D) cluster, with a coordinate given by the strips' center of gravity and an uncertainty corresponding to the number of strips. These 1D clusters on the orthogonal readout planes in a single RPC module are paired into 2D hits, with an in-plane coordinate given by the intersection of the two 1D coordinates and an in-plane error ellipse aligned along the two readout directions. A three-dimensional space point for each 2D hit is constructed from the in-plane coordinate and prior

knowledge of the position and normal vector of the module's median plane. The module alignment is accomplished with surveys and then refined to 1 mm accuracy by reconstruction of cosmic rays and $e^+e^- \to \mu^+\mu^-$ events in the CDC and KLM.

On rare occasions (~ 1 %), more than one 1D cluster of the same readout direction appears in an RPC module. Then ghost 2D hits are fabricated from the false intersections of such clusters with those in the orthogonal view.

3.4 Track-hit association

For each crossing of a KLM layer by the extrapolated track, 2D hits in that layer are associated with the track if they are within 25 cm or 5σ of the crossing point, whichever is greater. Sharing of 2D hits with two or more tracks is negligible: < 0.1 % among the tracks identified as muons in hadronic events. The track crossing increments the predicted range of the track by one layer, while the discovery of an associated hit increments the measured range. If the extrapolated crossing of the layer is in the inter-module gap and no associated 2D hit is found in the neighboring modules, then the track is deemed to have missed that layer so that neither its predicted nor measured ranges are incremented. Thus, the outermost layer that is crossed by the extrapolation or that has an associated hit defines the track's predicted or measured range, respectively—even if it escapes from the detector.

3.5 Pre-selection

To save a considerable amount of CPU time in the re-extrapolation of tracks through the KLM in the next stage of the analysis, tracks are "pre-selected" based on the available information. A track must have associated hits in at least two KLM superlayers, and its predicted and measured ranges must differ by no more than five layers. Tracks that fail this requirement are tagged with a goodness of fit (χ^2_r) value of zero, and are not re-extrapolated in the next pass. Thus, only the first-pass estimates of the predicted and measured ranges are used to test the muon hypothesis for such tracks.

Approximately 90% of the pions and 4.5% of the muons within the KLM acceptance fail this pre-selection (Fig.3). The failing muons typically pass in or near the cracks within the KLM acceptance (Fig.4). The peaks in Fig. 3 correspond to the gaps between modules at the octant (quadrant) boundaries in the barrel (endcap). The enhancement at 50-100° in the barrel is due to the dead space occupied by the liquid helium chimney of the superconducting solenoid's cryogenic system. The variation in peak height in Fig. 3(b) arises from the different gap spacings between endcap quadrants.

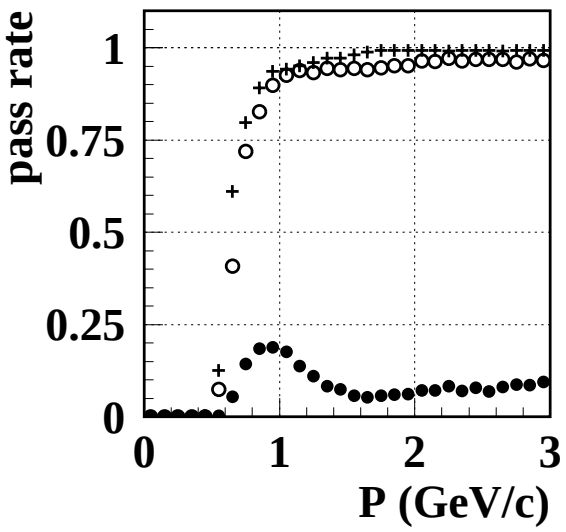

Figure 3: *Preselection's pass rate for muons (open circle) and pions (closed circle) with polar angles between* 23° *and* 150°. *The crosses show the fraction of muons with at least one associated KLM hit.*

3.6 Re-extrapolation of track

The tracks that have been preselected are re-extrapolated layer by layer through the KLM by GEANT3—now assuming that the track is a muon—using Kalman filtering and fitting.[10] Hits in a KLM layer are once again associated with the track if they are within either 25 cm or 5σ of the re-extrapolated crossing point. A track crossing of the plane within an inter-module gap is treated as before.

In this re-extrapolation, the associated hits in preceding KLM layers provide feedback to

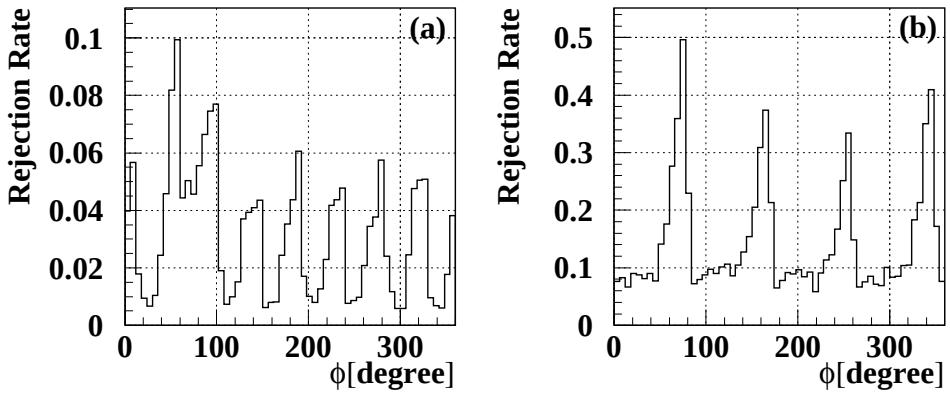

Figure 4: *Distributions of prerejected single-track simulated muons (μ^-, $1.0 < p < 3.0$ GeV/c) in (a) the barrel and (b) the endcaps.*

steer the track extrapolation to the next layer. The Kalman filtering/fitting process accounts for the growth in transverse deviations (σ) due to multiple scattering and ionization energy loss as well as this steering of the re-extrapolated track. The explicit formulae used in this process are given in reference [11].

3.7 Muon likelihood

Two quantities are used to test the hypothesis that a track is a muon rather than a hadron. These are ΔR, the difference between the measured and expected range of the track, and χ^2_r, the goodness of fit of the transverse deviations of all hits associated with the track (normalized by the number of hits). Figure 5 shows ΔR and χ^2_r for pre-selected tracks of simulated events containing a single muon or pion.

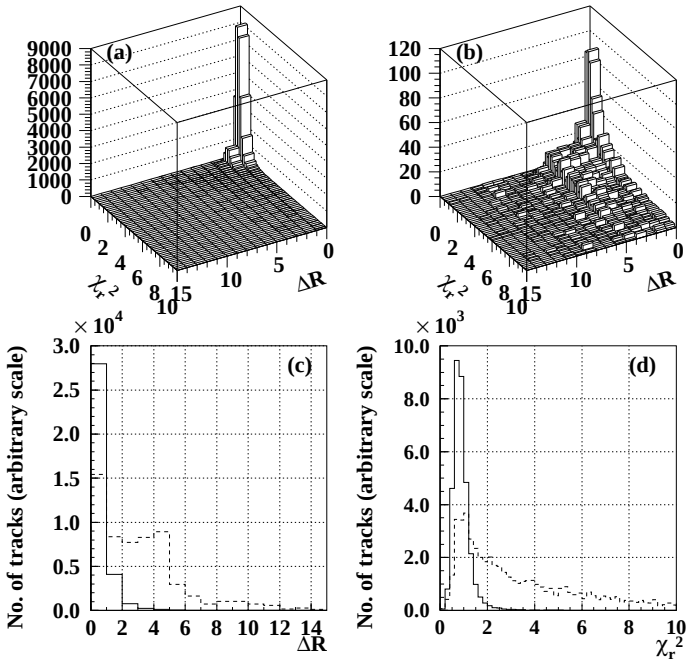

Figure 5: *ΔR and χ_r^2 for pre-selected Monte Carlo single muons and pions. ΔR vs. χ_r^2 for (a) single muons, (b) single pions. (c) ΔR, (d) χ_r^2 for muons (solid) and pions (dashed).*

Probability density distributions of ΔR and χ_r^2 are constructed beforehand using simulated single-track events containing a muon, pion, or kaon. Since the observed range difference and normalized transverse deviations are known to be uncorrelated or at worst very weakly correlated, the joint probability density is a product of these separate probability densities: $p(\Delta R, \chi_r^2) = p_1(\Delta R) \cdot p_2(\chi_r^2)$. Recall that pre-rejected tracks have $\chi_r^2 \equiv 0$ so that no discrimination based on this variable is possible for such tracks.

In-acceptance tracks—crossing at least one KLM layer—are classified according to whether they are predicted to stop in or escape from either the barrel or endcap KLM. For a given

track, characterized by ΔR, χ^2_r and this classification, the probability densities p_μ, p_π and p_K for muons, pions, and kaons, respectively, are obtained from the distributions that had been constructed earlier. The likelihood $p_\mu/(p_\pi + p_K)$ of the track being a muon rather than a hadron extends from 0 to ∞; for convenience, we use instead the normalized muon likelihood $\mathcal{L}_\mu = p_\mu/(p_\mu + p_\pi + p_K)$. Figure 6 shows the muon detection efficiency and the pion fake rate as a function of the cut on $\mathcal{L}_\mu$ for simulated single-track events. The muon detection efficiency starts to drop dramatically if the cut is placed higher than 0.9, so we choose $\mathcal{L}_\mu > 0.9$ as the standard cut to identify muons. For the physics channels that require higher muon detection efficiency at the price of higher pion fake rate, we use the looser cut of $\mathcal{L}_\mu > 0.1$. In the next section, we present the performance for both cuts.

4 Performance

We characterize the muon identification method by the muon detection efficiency and hadron fake rate. Fake muons are mostly punch-through and decay-in-flight pions or kaons. These measures vary with momentum and the region of the KLM traversed by the particle. They do not depend noticeably on the particle charge, but are degraded little by track density.

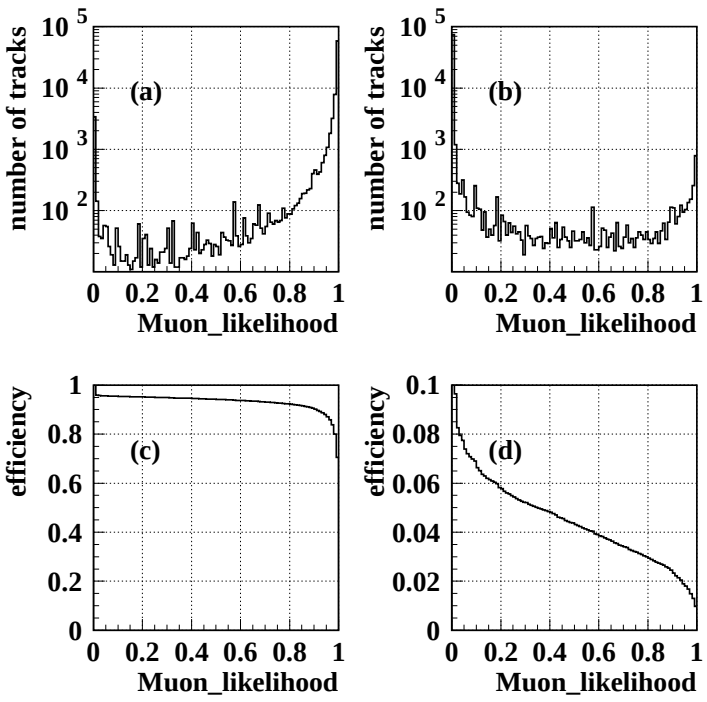

Figure 6: *Normalized muon likelihood for Monte Carlo single muons and pions. (a)(c) single muons, (b)(d) single pions.*

4.1 Muon Detection Efficiency

High purity muons are obtained with the two photon reaction, $e^+e^- \to e^+e^-\mu^+\mu^-$, by tagging one of the muons with a high muon likelihood and then examining the other minimum-ionizing track in the event. These muon candidates cover the momentum region of interest (0.6–3.0 GeV/c) and the KLM acceptance ($25^\circ < \theta < 145^\circ$). The selection criteria are enumerated in Appendix A-1. The momentum and polar angle distributions of the candidates are shown in Fig. 7, for 21.5 pb^{-1} of data collected between January and July, 2001. The purity of the

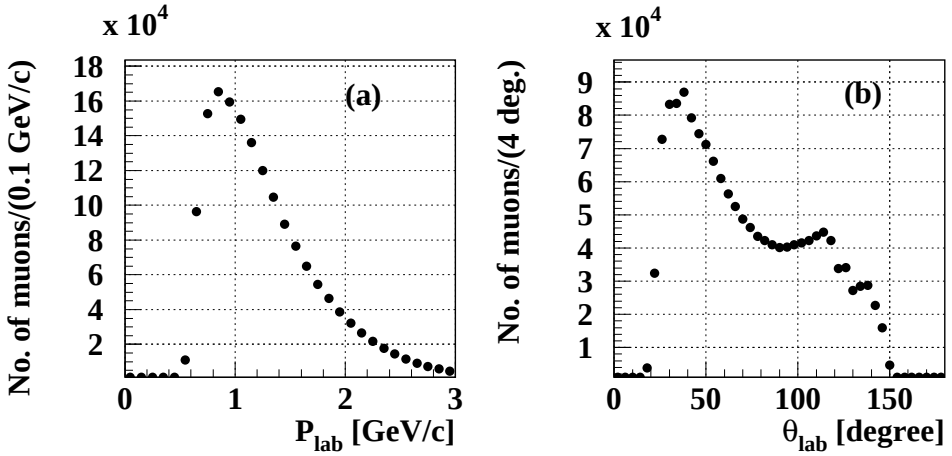

Figure 7: *Distributions of (a) momentum and (b) polar angle of the muons in* $e^+e^- \to e^+e^-\mu^+\mu^-$*, used for the efficiency measurements. The other muons of the pairs are tagged by very strict muon condition* ($\mathcal{L}_\mu > 0.99$)*.*

muon sample is 97.8%, estimated by simulation. The contamination is predominantly from $e^+e^- \to \tau^+\tau^-$ where one τ decays leptonically to give a tag muon and the other decays to $\pi\nu$ to give a fake-muon candidate (1.6%), or from $e^+e^- \to e^+e^-\pi\pi X$ where one of the pions is falsely tagged as a muon (0.6%).

The measured efficiencies are shown as a function of momentum in Fig. 8 for $\mathcal{L}_\mu > 0.9$ and $\mathcal{L}_\mu > 0.1$, for the KLM barrel only and for the entire KLM acceptance. The efficiencies have a threshold of about 0.7 GeV/c and a plateau above 1.0 GeV/c. In the plateau region of 1.0–3.0 (1.5–3.0) GeV/c, the full-acceptance efficiency is $88.8 \pm 0.9\%$ ($89.6 \pm 1.0\%$) for $\mathcal{L}_\mu > 0.9$ and $92.5 \pm 0.8\%$ ($92.7 \pm 0.9\%$) for $\mathcal{L}_\mu > 0.1$. The efficiencies as a function of polar and azimuthal angle are shown in Fig. 9 for the 1.0–3.0 GeV/c candidates.

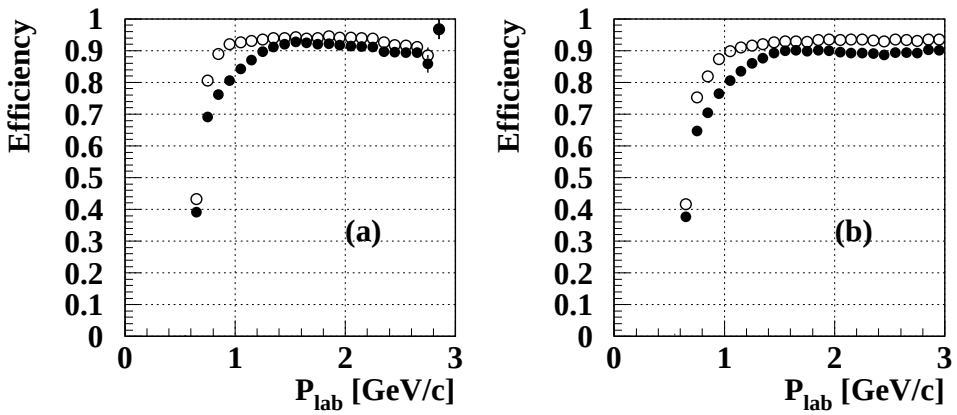

Figure 8: *Measured efficiency of muon identification as a function of momentum, measured by* $e^+e^- \to e^+e^-\mu^+\mu^-$*: (a) barrel* ($51^\circ < \theta < 117^\circ$)*, (b) whole polar angle region* ($25^\circ < \theta < 145^\circ$)*, for* $\mathcal{L}_\mu > 0.9$ *(closed circles) and* $\mathcal{L}_\mu > 0.1$ *(open circles).*

The momentum ranges 1.0–3.0 GeV/c and 1.5–3.0 GeV/c correspond to the regions of approximately constant muon detection efficiency and pion fake rate, respectively. The errors are statistical. The systematic uncertainty is estimated to be 2%, mainly from the residual hadron contamination in the muon sample and also from the process of integrating the p and θ distributions.

The ratio of the efficiencies for positively- to negatively-charged candidates within the entire KLM acceptance is shown in Fig. 10 as a function of momentum. This ratio is consistent with 1.0 within the systematic error.

Track density affects the muon identification efficiency through the degradation in the

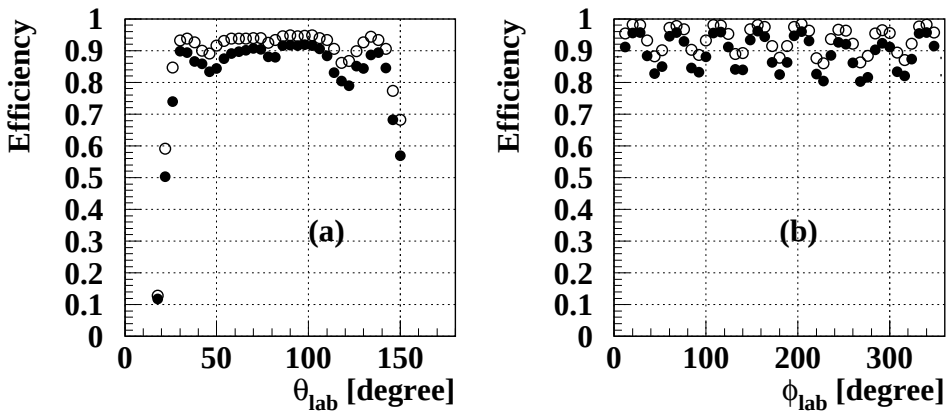

Figure 9: *Measured efficiency of muon identification vs polar angle and azimuthal angle, measured by* $e^+e^- \to e^+e^-\mu^+\mu^-$*: (a) polar angle,* ($1.0 < p < 3.0$ *GeV/c), (b) azimuthal angle,* ($1.0 < p < 3.0$ *GeV/c, barrel), for* $\mathcal{L}_\mu > 0.9$ *(closed circles) and* $\mathcal{L}_\mu > 0.1$ *(open circles).*

CDC track reconstruction performance under high track density conditions. We studied this effect in two ways: by overlaying a simulated single-track muon on a hadronic event taken from real data and then analyzing many such high track density events, and by using $J/\psi \to \mu^+\mu^-$ decays in $B\overline{B}$ events.

The measured efficiencies over the entire KLM acceptance for 1.0–3.0 (1.5–3.0) GeV/c muons in the hybrid events are $88.7 \pm 0.3\%$ ($89.3 \pm 0.4\%$) for $\mathcal{L}_\mu > 0.9$, and $93.4 \pm 0.3\%$ ($93.7 \pm 0.3\%$) for $\mathcal{L}_\mu > 0.1$. These numbers are approximately 1 % lower than the ones for simulated single-track muons.

The measured efficiencies from the $J/\psi \to \mu^+\mu^-$ decays in $B\overline{B}$ events over the entire KLM

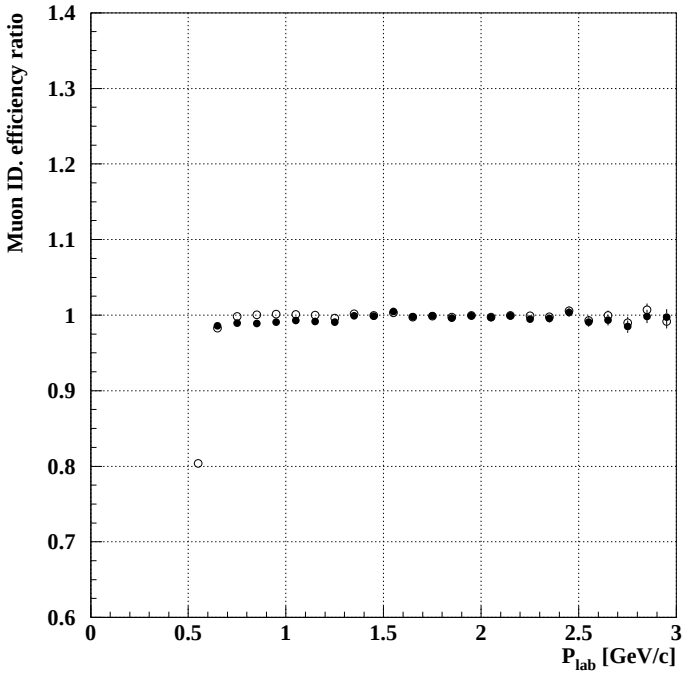

Figure 10: *Ratio of the efficiencies for positive to negative muon candidates obtained from* $e^+e^- \to e^+e^-\mu^+\mu^-$*, for* $\mathcal{L}_\mu > 0.9$ *(closed circles) and* $\mathcal{L}_\mu > 0.1$ *(open circles).*

acceptance are $90.1 \pm 1.1\%$ for $\mathcal{L}_\mu > 0.9$ and $93.8 \pm 1.2\%$ for $\mathcal{L}_\mu > 0.1$. These are consistent with the values obtained from the hybrid events. In this case, we used the yields of double-tagged (N_2) and single-tagged (N_1) J/ψ mesons [2] to calculate the efficiency $\varepsilon = 2X/(1+X)$, where $X = N_2/N_1$. The yields were obtained by fitting the J/ψ peaks in the $\mu^+\mu^-$ invariant mass distributions, as shown in Fig. 11.

[2] For the single-tag mesons, the other daughter track was required to extrapolate through at least one KLM layer.

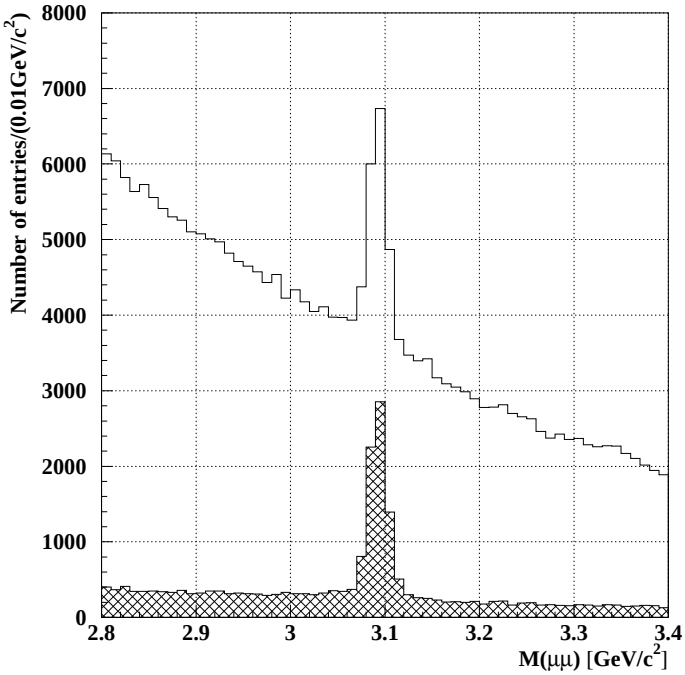

Figure 11: *Invariant mass distribution of $\mu^+\mu^-$ for single-tagged (open) and double-tagged (shaded) cases ($\mathcal{L}_\mu > 0.9$). J/ψ peak is seen at 3.1 GeV/c^2.*

4.2 Fake Rates

The majority of fake muons are punch-through or decay-in-flight pions and kaons. Of all decay-in-flight hadrons, approximately half the pions and most of the kaons have a disagreement between their predicted and measured ranges. For example, 2-3% of the 1 GeV/c pions produced at the origin decay before reaching ECL. Among these, the ones that decay outside the CDC have daughter muons with smaller momentum—roughly half of p_π—so they will range out sooner than the prediction based on p_π. Consequently, between 20% (at 2 GeV/c)

and 60% (at 1 GeV/c) of simulated decay-in-flight pions are rejected by requiring $\mathcal{L}_\mu > 0.9$. The decay-in-flight hadrons that survive such a cut, as well as those that neither decay nor suffer an inelastic hadronic interaction, are classified as fakes.

We measure the fake rate using the pions from $K_S \to \pi^+\pi^-$ and the kaons from $D \to K\pi$ where the D meson is identified by selecting observing the slow pion in $D^* \to D\pi_{\rm slow}$.

4.2.1 Pion fake rate

We select charged pions from $K_S \to \pi^+\pi^-$ in an 11.9 pb^{-1} hadronic event sample recorded between April and July 2001, using the selection criteria listed in Appendix A-2. The purity of the sample was estimated to be 97.96%, obtained by simulation. Of the impurity, muons accounted for 0.19%, and K, p, and e the remaining 1.85%. The momentum and polar angle distributions of the pions are shown in Fig. 12. The bias of the cut on the $\pi^+\pi^-$ invariant mass to perhaps exclude decay-in-flight pions was studied by simulation and found to affect the fake rate by less than 0.2%.

The measured fake rates as a function of momentum are shown in Fig. 13 for $\mathcal{L}_\mu > 0.9$ (0.1), presented separately for the pions in the KLM barrel and those in the entire acceptance. The fake rates are approximately constant at momenta above 1.5 GeV/c. In the momentum region 1.0–3.0 (1.5–3.0) GeV/c, the fake rate over the entire acceptance is $1.35 \pm 0.07\%$

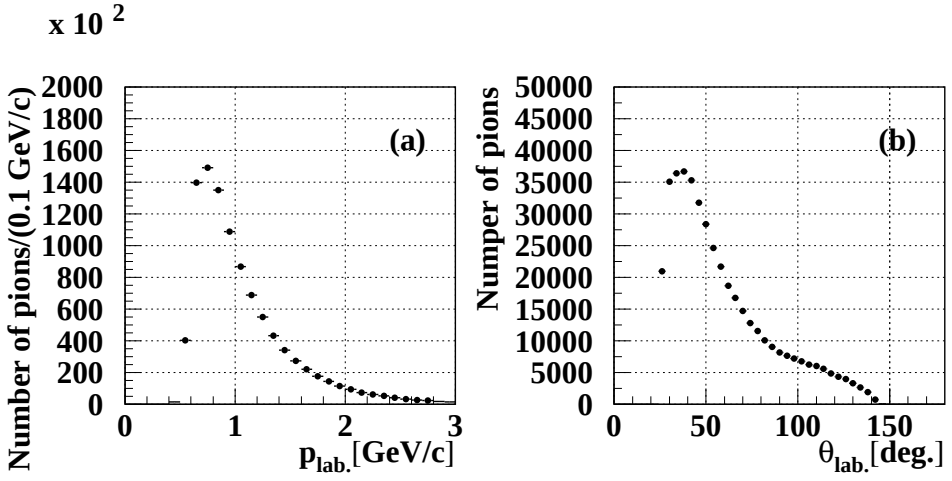

Figure 12: *Distributions of (a) momentum and (b) polar angle of the pions in* $Ks \to \pi^+\pi^-$, *used in the fake rate measurements.*

$(1.27 \pm 0.08\%)$ for $\mathcal{L}_\mu > 0.9$ and $2.76 \pm 0.09\%$ $(2.31 \pm 0.10\%)$ for $\mathcal{L}_\mu > 0.1$, respectively. The errors are statistical only. The polar and azimuthal angle dependences of the fake rates are shown in Fig. 14 for the 1.0–3.0 GeV/c pions.

The ratio of the fake rates for positively- to negatively-charged pions within the entire KLM acceptance is shown in Fig. 15 as a function of momentum for $\mathcal{L}_\mu > 0.9$ (0.1). This ratio is systematically larger than one because negative pions have a higher cross section for nuclear capture and are thus less likely to punch through.

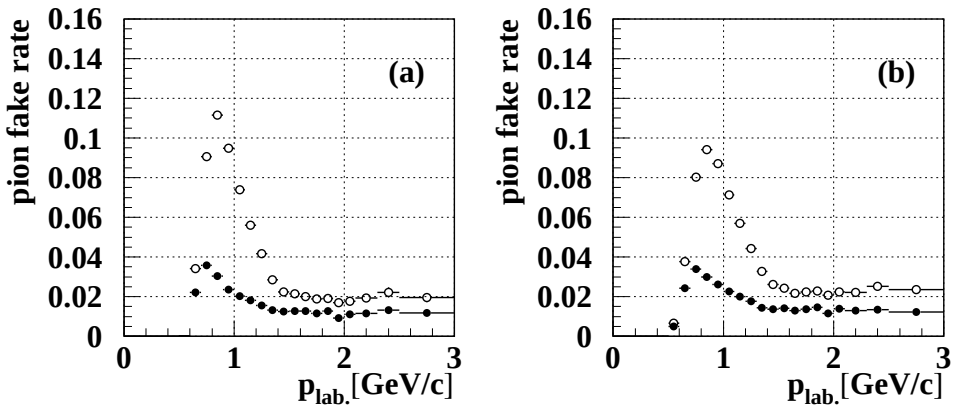

Figure 13: *Measured fake rate of pions vs momentum by* $Ks \to \pi^+\pi^-$*: (a) barrel, (b) whole polar angle region, for* $\mathcal{L}_\mu > 0.9$ *(closed circles) and* $\mathcal{L}_\mu > 0.1$ *(open circles).*

4.2.2 Kaon fake rate

To measure the kaon fake rate, we used a kaon sample from $D^0 \to K^-\pi^+$ and its charge conjugate in a 11.9 pb^{-1} event sample collected between April and July 2001. The selection criteria are listed in Appendix A-4. The purity of the selected kaons is estimated to be 97.7%. Most of the impurities are pions that combine accidentally to give the D^0 mass. Muon contamination is estimated to be less than 0.1%. The momentum and polar angle distributions of the kaons are shown in Fig. 16.

The measured fake rates of the kaons and the pions within the KLM barrel from $D^0 \to K^-\pi^+$ and its charge conjugate are shown in Fig. 17 as a function of momentum for $\mathcal{L}_\mu > 0.9$ and $\mathcal{L}_\mu > 0.1$. The measured kaon fake rate for 1.0–3.0 GeV/c kaons is $1.7 \pm 0.4\%$ ($3.3 \pm 0.8\%$)

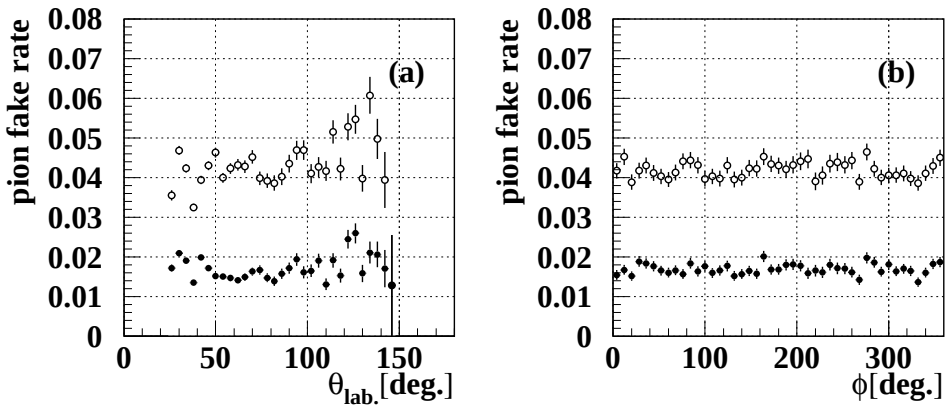

Figure 14: *Measured fake rate of pions vs polar and azimuthal angles by* $Ks \to \pi^+\pi^-$*: (a) polar angle (*$1.0 < p < 3.0$ *GeV/c), (b) azimuthal angle (*$1.0 < p < 3.0$ *GeV/c, barrel), for* $\mathcal{L}_\mu > 0.9$ *(closed circles) and* $\mathcal{L}_\mu > 0.1$ *(open circles).*

for $\mathcal{L}_\mu > 0.9$ (0.1). Application of the kaon veto, $\mathcal{L}_{\rm K} < 0.9$ (derived from measurements in the CDC, ACC, and TOF), rejects 90% of the punch-through kaons at 1 GeV/c, leaving the bulk (80∼90%) of the remaining fakes as decay-in-flight kaons. Use of this kaon veto also reduces the uncertainties in the kaon fake rate, dominated by the uncertainties in the simulation's hadronic cross sections, to a negligible level ($< 0.2\%$).

For decay-in-flight kaons, the track reconstruction program will find both the parent kaon and the daughter muon about 1/3 of the time for 1 GeV/c kaons. Thus, a cut on the track's closest approach to the z-axis ($dr < 2.0$ cm) reject about 90% of these separately reconstructed muon daughters. As a result, the kaon fake rate is halved for both $\mathcal{L}_\mu > 0.9$ and 0.1 by application of these two cuts. The corresponding reduction of the muon detection

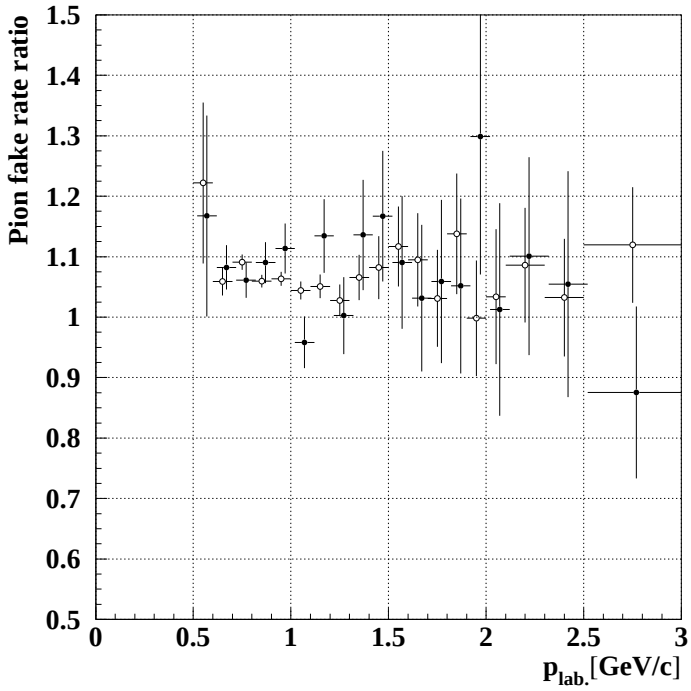

Figure 15: *The measured ratio (fake(+)/fake(−)) of pion fake rate for positive pions to negative pions, measured by* $Ks \to \pi^+\pi^-$ *for* $\mathcal{L}_\mu > 0.9$ *(closed circles) and* $\mathcal{L}_\mu > 0.1$ *(open circles).*

efficiency by the kaon veto is only 1% at 1 GeV/c and 2% at 2 GeV/c.

The fake rates for 1.0–3.0 GeV/c pion daughters within the KLM barrel from the same D^0 decays are 1.5% for $\mathcal{L}_\mu > 0.9$ and 2.8% for $\mathcal{L}_\mu > 0.1$. These are consistent with the measurements in section 4.2.1.

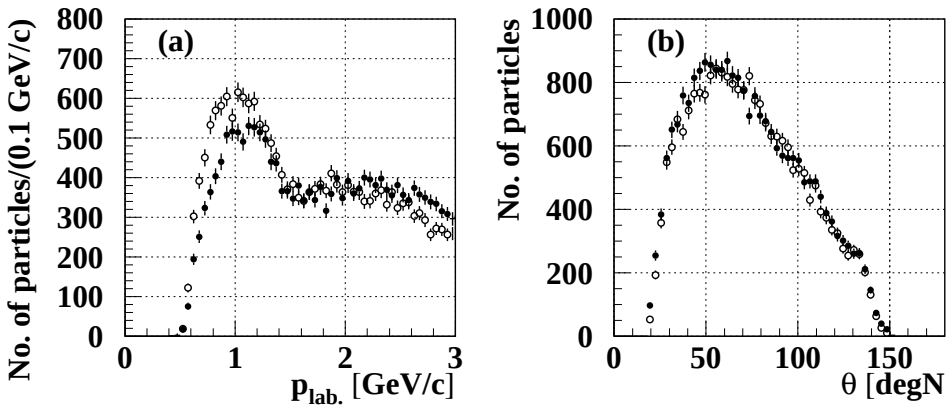

Figure 16: *Distributions of* (a) *momentum and (b) polar angle of the kaons (closed circles) and pions (open circles) from* $D \to K\pi$ *with Outcome* > 0.

5 Summary

Muon identification code was made, based on the algorithm that uses the difference of muons from hadrons in the range and the scattering of the particles in the KLM. The results of the identifications are given by probabilities, referred as $\mathcal{L}_\mu$, ranging from 0 to 1. We use $\mathcal{L}_\mu > 0.9$ for the standard selection and $\mathcal{L}_\mu > 0.1$ for higher efficiencies.

The measured efficiencies of muon identification and hadron fake rates are summarized in Table 1. The efficiencies were measured by the muons from two-photon reactions: $e^+e^- \to e^+e^-\mu^+\mu^-$. They shows a plateau in the region $p > 1.0$ GeV/c. The effect of track's crowdiness to the efficiency was studied by simulated single-track muons embedded in hadronic

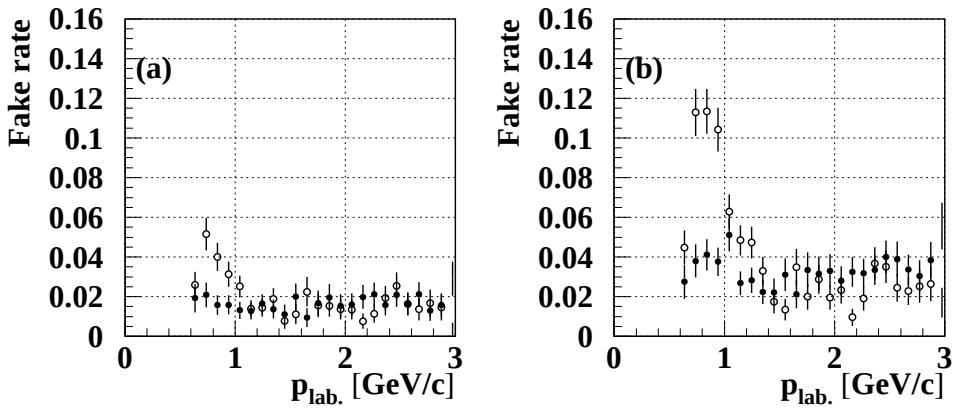

Figure 17: *Fake rate of the kaons (closed circles) and the pions (open circles) from* $D \to K\pi$ *for (a)* $\mathcal{L}_\mu > 0.9$ *and (b)* $\mathcal{L}_\mu > 0.1$.

events, and also by the muons from $J/\psi \to \mu^+\mu^-$. The effect was measured to be small (1%). The systematic uncertainty in the efficiencies is 2 %.

Fake rates of pions were measured using pions from $K_{\rm S}$. The rates are approximately constant in the region $p > 1.5$ GeV/c. Fake rates of kaons were measured using kaons from $D \to K\pi$. The rates are approximately constant (1.7 %) in momentum above threshold. These can be reduced to 0.8% by applying a cut on the kaon likelihood ($\mathcal{L}_K < 0.9$) and a cut on the closest approach distance of the track to the interaction point ($dr < 2.0$ cm).

Table 1: Efficiencies and fake rates. The errors are statistical.

source	efficiency [%]			
	1.0 - 3.0 GeV/c		1.5 - 3.0 GeV/c	
	$\mathcal{L}_\mu > 0.9$	$\mathcal{L}_\mu > 0.1$	$\mathcal{L}_\mu > 0.9$	$\mathcal{L}_\mu > 0.1$
$ee \to ee\mu\mu$	88.8 ± 0.9	92.5 ± 0.8	89.6 ± 1.0	92.7 ± 0.9
hybrid	88.7 ± 0.3	93.4 ± 0.3	89.3 ± 0.4	93.7 ± 0.3
$J/\psi \to \mu\mu$	90.1 ± 1.1		93.8 ± 1.2	

source	fake rate [%]			
	1.0 - 3.0 GeV/c		1.5 - 3.0 GeV/c	
	$\mathcal{L}_\mu > 0.9$	$\mathcal{L}_\mu > 0.1$	$\mathcal{L}_\mu > 0.9$	$\mathcal{L}_\mu > 0.1$
pion ($K_s \to \pi\pi$)	1.35 ± 0.07	2.76 ± 0.09	1.27 ± 0.08	2.31 ± 0.10
kaon ($D \to K\pi$)	1.7 ± 0.4	3.3 ± 0.8		

6 Acknowledgement

We thank all the other Belle collaborators, especially the members of the KLM subdetector, for building and operating the hardware and software. This work was supported by the Ministry of Education, Culture, Sports, Science and Technology of Japan, the U.S.-Japan Corporative Research Program in High Energy Physics, and the U.S. Department of Energy.

Appendix Selection Criteria

The selection criteria, used in this report, are listed below. The asterisks indicate the variables in the center-of-mass system.

A-1 $e^+e^- \to e^+e^-\mu^+\mu^-$ **process**

To select two-photon events, $e^+e^- \to (e^+e^-)\mu^+\mu^-$, we select two-charged-track events by the following conditions.

1. Two charged tracks: $N_{\rm track} = 2$ with $p_{\rm t} > 0.3$ GeV/c.
2. Net charge: $\sum Q = 0$.
3. $|\sum \vec{p}_{\rm t}| < 0.2$ GeV/c.
4. $\sum E < 6$ GeV, where $\sum E$ is a scaler sum of the cluster energies.
5. $\sum |p| < 6$ GeV/c, where $\sum |p|$ is a scaler sum of the track momenta.

where the variables are in the laboratory frame. Then, the $e^+e^- \to e^+e^-e^+e^-$ contaminations are removed by applying electron identification to the tracks. Furthermore, cosmic-rays are rejected by applying a cut on two-track collinearity in the polar angle ($|\Delta\theta - \pi| < 0.1$

rad). To reject $e^+e^- \to (e^+e^-)\pi^+\pi^-$ background, we tag one of the tracks as a muon with a very tight muon selection ($L_\mu > 0.99$). In addition, we require that the tagged track has to have small proton probability, and also the track has to be in the good momentum and polar angle regions of muon identification ($p > 0.7$ GeV/c, $30^\circ < \theta < 140^\circ$).

A-2 $K_s \to \pi\pi$ **process**

To select $K_{\rm S}$, we select hadronic events using the following criteria.

1. $N_{\rm good} \geq 5$, where $N_{\rm good}$ is a number of "good tracks". A good track is selected by $p_{\rm t} > 0.1$ GeV/c, $dr < 2.0$ cm and $|dz| < 4.0$ cm at the closest distance to the interaction point.

2. $\sum E^* + \sum |p^*| \geq 0.5\sqrt{s}$ in the rest frame, where $\sum |p^*|$ is a scaler sum of momentum and $\sqrt{s}$ is the center-of-mass energy.

3. $|\sum E^*_{\rm z} + \sum p^*_{\rm z}| \leq 0.5\sqrt{s}$.

4. $|\sum p^*_{\rm z}| \leq 0.3\sqrt{s}$.

5. $0.1 \leq \sum E_{\rm ECL} / \sum E \leq 0.8$, where $E_{\rm ECL}$ is the deposited energy in ECL.

6. $N_{\rm cluster}({\rm ECL}) > 1$ with $E_{\rm ECL} > 0.1$ GeV and $-0.7 < \cos\theta < 0.9$.

7. Primary event vertex: $r_{\rm v} < 1.5$ cm and $|z_{\rm v}| < 3.5$ cm.

After this, we select pairs of oppositely charged tracks ("vee"s) from $K_{\rm S}$ decays by the following criteria.

1. $|\Delta z| < 0.5$ cm, where $|\Delta z|$ is the distance in the z direction between the two tracks at the vee's vertex.
2. $r_{\rm vtx} < 5$ cm, where $r_{\rm vtx}$ is the radial distance of the vee's vertex from the interaction point.
3. $|\Delta\phi| < 15^\circ$, where $|\Delta\phi|$ is the deflection angle, which is the opening angle between the vee's vertex direction from the interaction point and the direction of the vector sum of the two track's momenta.
4. $|m(\pi\pi) - m(K_{\rm S})| < 3\sigma$, where $\sigma = 0.025$ GeV/c^2.

A-4 $D \to K\pi$ **via** $D^* \to D\pi_S$

To select kaons from $D^* \to D\pi_S$ followed by $D \to K\pi$, we select hadronic events described in A-2. Then, we apply

1. $|m(K\pi) - m(D^0)| \leq 0.030$ GeV/c^2
2. $|m(K'\pi') - m(D^0)| \geq 0.030$ GeV/c^2

3. $|\cos\theta_D| \leq 0.8$

4. $p^*_{D*}/E^{CM}_{\rm beam} \geq 0.5$

5. $|m(K\pi\pi) - m(K\pi)| \leq 1.5$ MeV/c^2

where K' and π' are flipped assignements of kaon and pion, and $\cos\theta_D$ is the decay angle of D, defined as the angle of the K momentum in the D rest frame with respect to the D momentum in the center-of-mass system (CMS), and p^*_{D*} and $E^{CM}_{\rm beam}$ are the D^* momentum and the beam energy in the CMS, respectively.

References

[1] Belle Collaboration, A. Abashian *et al.*, *The Belle Detector*, KEK Report 2000-4, to be published in Nucl. Instr. and Meth.

[2] KEKB B Factory Design Report, KEK Report 95-1, 1995.

[3] Belle Collaboration, K. Abe *et al.*, Phys. Rev. Lett. **87**, 091802 (2001).

[4] A.B. Carter and A.I. Sanda, Phys. Rev. **D23**, 1567 (1981); I.I. Bigi and A.I. Sanda, Nucl. Phys. **B193**, 85 (1981).

[5] A. Abashian *et al.*, Nucl. Instr. and Meth. **A449**, 112 (2000).

[6] S. Uno, Nucl. Instr. and Meth. **A379**, 421 (1996); K. Emi *et al.*, Nucl. Instr. and Meth. **A379**, 225 (1996); S. Uno *et al.*, Nucl. Instr. and Meth. **A330**, 55 (1993); H. Hirano *et al.*, Nucl. Instr. and Meth. **A455**, 294 (2000); M. Akatsu *et al.*, Nucl. Instr. and Meth. **A454**, 322 (2000).

[7] H. Ikeda *et al.*, Nucl. Instr. and Meth. **A441**, 401 (2000).

[8] R. Brun *et al.*, GEANT 3.21, CERN Report No. DD/EE/84-1 (1987).

[9] R.F. Holsinger and C. Iselin, "The CERN-POISSON Program Package (POISCR) User Guide", Geneva, Auguest, 1984.

[10] R.E. Kalman, Trans. ASME, J. Basic Eng., **82**, pp.35-45 (1960); R. Frühwirth, Nucl.

Instr. and Meth. **A262**, 444 (1987); R. Harr, IEEE trans. Nucl. Sci., vol. 42, pp. 134-147 (1995).

[11] Y. Teramoto, Nucl. Instr. and Meth. **A449**, 344 (2000).